Convergence of the dominant pole algorithm and Rayleigh quotient iteration

by

Joost Rommes and Gerard L.G. Sleijpen

Convergence of the dominant pole algorithm and Rayleigh quotient iteration

Joost Rommes* and Gerard L.G. Sleijpen

September, 2006

Abstract

The dominant poles of a transfer function are specific eigenvalues of the state space matrix of the corresponding dynamical system. In this paper, two methods for the computation of the dominant poles of a large scale transfer function are studied: two-sided Rayleigh Quotient Iteration (RQI) and the Dominant Pole Algorithm (DPA). Firstly, a local convergence analysis of DPA will be given, and the local convergence neighborhoods of the dominant poles will be characterized for both methods. Secondly, theoretical and numerical results will be presented that indicate that for DPA the basins of attraction of the dominant pole are larger than for two-sided RQI. The price for the better global convergence is only a few additional iterations, due to the asymptotically quadratic rate of convergence of DPA, against the cubic rate of two-sided RQI.

1 Introduction

The transfer function of a large scale dynamical system often only has a small number of dominant poles compared to the number of state variables. The dominant behavior of the system can be captured by projecting the state space on the subspace spanned by the eigenvectors corresponding to the dominant poles. This type of model reduction is known as modal approximation, see for instance [23]. The computation of the dominant poles, that are specific eigenvalues of the system matrix, and the corresponding modes, requires specialized eigenvalue methods.

In [10] Newton's method is used to compute a dominant pole of single input single output (SISO) transfer function: the Dominant Pole Algorithm (DPA). In two recent publications this algorithm is improved and extended to a robust and efficient method for the computation of the dominant poles, modes and modal approximates of large scale SISO [17] and MIMO transfer functions [16].

This paper is concerned with the convergence behavior of DPA. Firstly, DPA will be related to two-sided or generalized Rayleigh quotient iteration [13, 15]. A local convergence analysis will be given, showing the asymptotically quadratic rate of convergence. Furthermore, for systems with a symmetric state-space matrix, a characterization of the local convergence neighborhood of the dominant pole will be presented for both DPA and RQI. The results presented in this paper are sharper than the results by Ostrowski [12, 13] and Beattie and Fox [4]. Secondly, theoretical and numerical results indicate that for DPA the basins of attraction of the most dominant poles are larger than for two-sided RQI. In practice, the asymptotically quadratic (DPA) instead of cubic rate (two-sided RQI) of convergence costs about two or three iterations.

The outline of this paper is as follows. Definitions and properties of transfer functions and dominant poles, and further motivation are given in section 2. The Dominant Pole Algorithm and its relation to two-sided Rayleigh quotient iteration are discussed in section 3. In section 4 the local convergence of DPA is analyzed. The basins of attraction of DPA and two-sided RQI are studied in section 5. Section 6 concludes.

---

*Mathematical Institute, Utrecht University, POBox 80010, 3508 TA, Utrecht, The Netherlands, http://www.math.uu.nl/people/rommes, `rommes@math.uu.nl`

2 Transfer functions, poles, and zeros

The motivation for this paper comes from dynamical systems $(E, A, \mathbf{b}, \mathbf{c}, d)$ of the form

$$\begin{cases} E\dot{\mathbf{x}}(t) &= A\mathbf{x}(t) + \mathbf{b}u(t) \\ y(t) &= \mathbf{c}^*\mathbf{x}(t) + du(t), \end{cases} \tag{1}$$

where $A, E \in \mathbb{R}^{n \times n}$, E may be singular, $\mathbf{b}, \mathbf{c}, \mathbf{x}(t) \in \mathbb{R}^n$, $u(t), y(t), d \in \mathbb{R}$. The vectors $\mathbf{b}$ and $\mathbf{c}$ are called the input, and output vector, respectively. The transfer function $H : \mathbb{C} \longrightarrow \mathbb{C}$ of (1) is defined as

$$H(s) = \mathbf{c}^*(sE - A)^{-1}\mathbf{b} + d. \tag{2}$$

The poles of transfer function (2) are a subset of the eigenvalues $\lambda_i \in \mathbb{C}$ of the matrix pencil (A, E). An eigentriplet $(\lambda_i, \mathbf{v}_i, \mathbf{w}_i)$ is composed of an eigenvalue λ_i of (A, E) and corresponding right and left eigenvectors $\mathbf{v}_i, \mathbf{w}_i \in \mathbb{C}^n$ (identified by their components in $\mathbf{b}$ and $\mathbf{c}$):

$$\begin{aligned} A\mathbf{v}_i &= \lambda_i E\mathbf{v}_i, & \mathbf{v}_i \neq 0, \\ \mathbf{w}_i^*A &= \lambda_i \mathbf{w}_i^*E, & \mathbf{w}_i \neq 0. \end{aligned}$$

Assuming that the pencil is non-defective, the right and left eigenvectors corresponding to finite eigenvalues can be scaled so that $\mathbf{w}_i^*E\mathbf{v}_i = 1$. Furthermore, it is well known that left and right eigenvectors corresponding to distinct eigenvalues are E-orthogonal: $\mathbf{w}_i^*E\mathbf{v}_j = 0$ for $i \neq j$. The transfer function $H(s)$ can be expressed as a sum of residues $R_i \in \mathbb{C}$ over the $\tilde{n} \leq n$ finite first order poles [9]:

$$H(s) = \sum_{i=1}^{\tilde{n}} \frac{R_i}{s - \lambda_i} + R_\infty + d, \tag{3}$$

where the residues R_i are

$$R_i = (\mathbf{c}^*\mathbf{v}_i)(\mathbf{w}_i^*\mathbf{b}),$$

and R_∞ is the constant contribution of the poles at infinity (often zero).

Although there are different indices of modal dominance [2, 7, 17, 23], the following will be used in this paper.

Definition 2.1. A pole λ_i of $H(s)$ with corresponding right and left eigenvectors $\mathbf{v}_i$ and $\mathbf{w}_i$ ($\mathbf{w}_i^*E\mathbf{v}_i = 1$) is called *the* dominant pole if $|R_i| > |R_j|$, for all $j \neq i$.

More generally, a pole λ_i is called dominant if $|R_i|$ is not very small compared to $|R_j|$, for all $j \neq i$. A dominant pole is well observable and controllable in the transfer function. This can also be seen in the corresponding Bode-plot (see fig. 1), which is a plot of $|H(i\omega)|$ against $\omega \in \mathbb{R}$: peaks occur at frequencies ω close to the imaginary parts of the dominant poles of $H(s)$. An approximation of $H(s)$ that consists of $k < n$ terms with $|R_j|$ above some value, determines the effective transfer function behavior [19] and is also known as transfer function modal equivalent:

$$H_k(s) = \sum_{j=1}^{k} \frac{R_j}{s - \lambda_j} + d.$$

The dominant poles are specific (complex) eigenvalues of the pencil (A, E) and usually form a small subset of the spectrum of (A, E). They can be located anywhere in the spectrum, see also figure 1. The two algorithms to compute poles (eigenvalues) that will be discussed in this paper, the Dominant Pole Algorithm (DPA) and two-sided Rayleigh Quotient Iteration (two-sided RQI), both start with an initial shift s_0, but behave notably differently: as can be seen in figure 1, DPA converges to the most dominant pole for many more initial shifts than two-sided RQI (marked by circles and x-es, respectively). In section 5 more of such figures will be presented and for all figures it holds: the more circles (compared to x-es), the better the performance of DPA over two-sided RQI. The typical behavior of DPA will be discussed in more detail in sections 4 and 5.

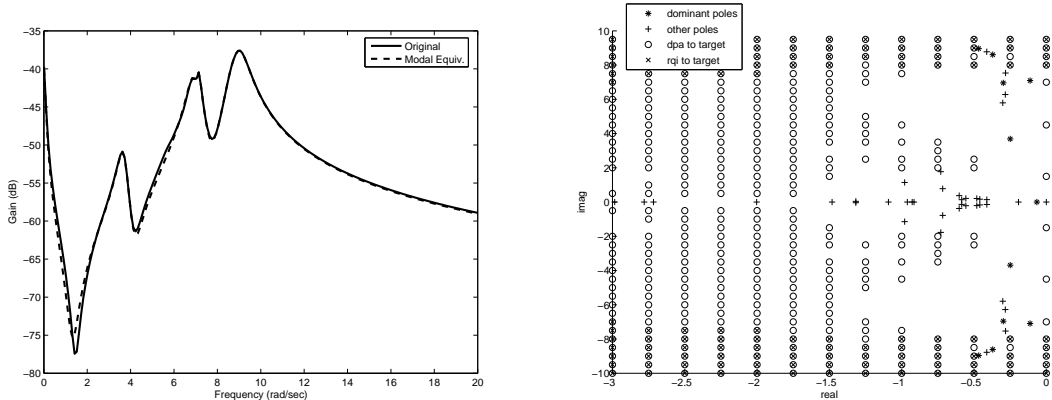Since the dominance of a pole is independent of d, without loss of generality $d = 0$ in the following.

Figure 1: The left figure shows the Bode plot of the transfer function ($n = 66$ states) of the New England test system [10], together with the Bode plot of the $k = 11$th order modal equivalent, constructed by projecting the system onto the modes of the 6 most dominant poles, which may belong to complex conjugated pairs. The right figure shows part of the pole spectrum together with the initial shifts for which DPA (marked by circles) and two-sided RQI (x-es) converge to the most dominant pole $\lambda = -0.467 \pm 8.96i$.

3   The Dominant Pole Algorithm (DPA)

The poles of transfer function (2) are the $\lambda \in \mathbb{C}$ for which $\lim_{s \to \lambda} |H(s)| = \infty$. Consider now the function $G : \mathbb{C} \longrightarrow \mathbb{C}$

$$G(s) = \frac{1}{H(s)}.$$

For a pole λ of $H(s)$, $\lim_{s \to \lambda} G(s) = 0$. In other words, the poles are the roots of $G(s)$ and a good candidate to find these roots is Newton's method. This idea is the basis of the Dominant Pole Algorithm (DPA) [10] (and can be generalized to MIMO systems as well, see [11, 16]).

The derivative of $G(s)$ with respect to s is given by

$$G'(s) = -\frac{H'(s)}{H^2(s)}. \tag{4}$$

The derivative of $H(s)$ with respect to s is

$$H'(s) = -\mathbf{c}^*(sE - A)^{-1}E(sE - A)^{-1}\mathbf{b}. \tag{5}$$

Equations (4) and (5) lead to the following Newton scheme:

$$
\begin{aligned}
s_{k+1} &= s_k - \frac{G(s_k)}{G'(s_k)} \\
&= s_k + \frac{1}{H(s_k)}\frac{H^2(s_k)}{H'(s_k)} \\
&= s_k - \frac{\mathbf{c}^*(s_k E - A)^{-1}\mathbf{b}}{\mathbf{c}^*(s_k E - A)^{-1}E(s_k E - A)^{-1}\mathbf{b}},
\end{aligned} \tag{6}
$$

The formula (6) was originally derived in [5]. Using $\mathbf{x}_k = (s_k E - A)^{-1}\mathbf{b}$ and $\mathbf{y}_k = (s_k E - A)^{-*}\mathbf{c}$, the

Newton update (6) can also be written as the generalized two-sided Rayleigh quotient $\rho(\mathbf{x}_k, \mathbf{y}_k)$:

$$
\begin{aligned}
s_{k+1} &= s_k - \frac{\mathbf{c}^*(s_k E - A)^{-1}\mathbf{b}}{\mathbf{c}^*(s_k E - A)^{-1}E(s_k E - A)^{-1}\mathbf{b}} \\
&= \frac{\mathbf{c}^*(s_k E - A)^{-1}A(s_k E - A)^{-1}\mathbf{b}}{\mathbf{c}^*(s_k E - A)^{-1}E(s_k E - A)^{-1}\mathbf{b}}. \\
&= \frac{\mathbf{y}_k^* A \mathbf{x}_k}{\mathbf{y}_k^* E \mathbf{x}_k}.
\end{aligned}
$$

An implementation of this Newton scheme is represented in Alg. 1. It is also known as the Dominant Pole Algorithm [10].

Algorithm 1 The Dominant Pole Algorithm (DPA).

INPUT: System $(E, A, \mathbf{b}, \mathbf{c})$, initial pole estimate s_0, tolerance $\epsilon \ll 1$
OUTPUT: Dominant pole λ and corresponding right and left eigenvectors $\mathbf{v}$ and $\mathbf{w}$
1: Set $k = 0$
2: **while** not converged **do**
3:    Solve $\mathbf{x}_k \in \mathbb{C}^n$ from $(s_k E - A)\mathbf{x}_k = \mathbf{b}$
4:    Solve $\mathbf{y}_k \in \mathbb{C}^n$ from $(s_k E - A)^*\mathbf{y}_k = \mathbf{c}$
5:    Compute the new pole estimate

$$
s_{k+1} = s_k - \frac{\mathbf{c}^*\mathbf{x}_k}{\mathbf{y}_k^* E \mathbf{x}_k} = \frac{\mathbf{y}_k^* A \mathbf{x}_k}{\mathbf{y}_k^* E \mathbf{x}_k}
$$

6:    The pole $\lambda = s_{k+1}$ with $\mathbf{v} = \mathbf{x}_k$ and $\mathbf{w} = \mathbf{y}_k$ has converged if

$$
||A\mathbf{x}_k - s_{k+1}E\mathbf{x}_k||_2 < \epsilon
$$

7:    Set $k = k + 1$
8: **end while**

The two linear systems that need to be solved in step 3 and 4 of Alg. 1 can be efficiently solved using one LU-factorization $LU = s_k E - A$, by noting that $U^*L^* = (s_k E - A)^*$. In this paper it will be assumed that an exact LU-factorization is available, although this may not always be the case for real-life examples, depending on the size and condition of the system. If an exact LU-factorization is not available, one has to use inexact Newton schemes, such as inexact Rayleigh Quotient Iteration and Jacobi-Davidson style methods [18, 8, 20], a topic that is subject to ongoing research.

3.1   DPA and two-sided Rayleigh quotient iteration

The generalized two-sided Rayleigh quotient iteration is defined as follows:

Definition 3.1. The generalized two-sided Rayleigh quotient $\rho(\mathbf{x}, \mathbf{y})$ is given by [13, 15] $\rho(\mathbf{x}, \mathbf{y}) \equiv \rho(\mathbf{x}, \mathbf{y}, A, E) \equiv \mathbf{y}^* A\mathbf{x}/\mathbf{y}^* E\mathbf{x}$, provided $\mathbf{y}^* E\mathbf{x} \neq 0$.

The two-sided Rayleigh quotient iteration [13, 15] is shown in Alg. 2. The only difference with DPA is that the right hand sides in step 3 and 4 of Alg. 1 are kept fixed, while the right hand sides in step 4 and 5 of Alg. 2 are updated every iteration.

While the use of the fixed right hand sides drops the asymptotic convergence rate from cubic to quadratic, it is exactly this use of fixed right hand sides that causes the typical better convergence to dominant poles, as will be shown later. In that light the quadratic instead of cubic local convergence, that in practice only makes a small difference in the number of iterations, is even more acceptable. Moreover, based on techniques in [4, 21] one can switch from DPA to two-sided RQI in the final phase of the process, to save some iterations. However, such techniques are not considered in this paper, since the primary goal is to study the convergence behavior.

Algorithm 2 Two-sided Rayleigh quotient iteration.

INPUT: System $(E, A, \mathbf{b}, \mathbf{c})$, initial pole estimate s_0, tolerance $\epsilon \ll 1$

OUTPUT: Pole λ and corresponding right and left eigenvectors $\mathbf{v}$ and $\mathbf{w}$

1: $\mathbf{x}_0 = (s_0 E - A)^{-1} \mathbf{b}$, $\mathbf{y}_0 = (s_0 E - A)^{-*} \mathbf{c}$, and $s_1 = \rho(\mathbf{x}_0, \mathbf{y}_0)$

2: Set $k = 1$

3: **while** not converged **do**

4:     Solve $\mathbf{x}_k \in \mathbb{C}^n$ from $(s_k E - A)\mathbf{x}_k = E\mathbf{x}_{k-1}/\|\mathbf{x}_{k-1}\|_2$

5:     Solve $\mathbf{y}_k \in \mathbb{C}^n$ from $(s_k E - A)^*\mathbf{y}_k = E^*\mathbf{y}_{k-1}/\|\mathbf{y}_{k-1}\|_2$

6:     Compute the new pole estimate

$$s_{k+1} = \rho(\mathbf{x}_k, \mathbf{y}_k) = \frac{\mathbf{y}_k^* A \mathbf{x}_k}{\mathbf{y}_k^* E \mathbf{x}_k}$$

7:     The pole $\lambda = s_{k+1}$ has converged if

$$\|A\mathbf{x}_k - s_{k+1} E \mathbf{x}_k\|_2 < \epsilon$$

8:     Set $k = k + 1$

9: **end while**

---

4 Local convergence analysis

The generalized two-sided Rayleigh quotient (Def. 3.1) has some well known basic properties, see [13, 15]:

- Homogeneity: $\rho(\alpha\mathbf{x}, \beta\mathbf{y}, \gamma A, \delta E) = (\gamma/\delta)\rho(\mathbf{x}, \mathbf{y}, A, E)$ for $\alpha, \beta, \gamma, \delta \neq 0$.

- Translation Invariance: $\rho(\mathbf{x}, \mathbf{y}, A - \alpha E, E) = \rho(\mathbf{x}, \mathbf{y}, A, E) - \alpha$.

- Stationarity (all directional derivatives are zero): $\rho = \rho(\mathbf{x}, \mathbf{y}, A, E)$ is stationary if and only if $\mathbf{x}$ and $\mathbf{y}$ are right and left eigenvectors of (A, E), respectively, with eigenvalue ρ and $\mathbf{y}^* E \mathbf{x} \neq 0$.

4.1 Asymptotically quadratic rate of convergence

In [15, p. 689] it is proved that the asymptotic convergence rate of two-sided RQI is cubic for non-defective matrices. Along the same lines it can be shown that the asymptotic convergence rate of DPA is quadratic. For the eigenvalue, this also follows from the fact that DPA is an exact Newton method, but for the corresponding left and right eigenvectors the following lemma is needed, gives a useful expression for $(\rho_{k+1} - \lambda)$ (using $s_k \equiv \rho_k \equiv \rho(\mathbf{x}_k, \mathbf{y}_k, A, E)$ from now on).

Lemma 4.1. *Let $\mathbf{v}$ and $\mathbf{w}$ be right and left eigenvectors of (A, E) with eigenvalue λ, i.e. $(A - \lambda E)\mathbf{v} = 0$ and $\mathbf{w}^*(A - \lambda E) = 0$, and $\mathbf{w}^* E \mathbf{v} = 1$. Let $\tau_k, \omega_k \in \mathbb{C}$ be scaling factors so that the solutions $\mathbf{x}_k$ and $\mathbf{y}_k$ of*

$$(\rho_k E - A)\mathbf{x}_k = \tau_k \mathbf{b} \quad and \quad (\rho_k E - A)^* \mathbf{y}_k = \omega_k \mathbf{c} \tag{7}$$

are of the form

$$\mathbf{x}_k = \mathbf{v} + \mathbf{d}_k \quad and \quad \mathbf{y}_k = \mathbf{w} + \mathbf{e}_k, \tag{8}$$

where $\mathbf{w}^* E \mathbf{d}_k = \mathbf{e}_k^* E \mathbf{v} = 0$. Then with $\mathbf{u} \equiv (I - E\mathbf{v}\mathbf{w}^*)\frac{\mathbf{b}}{\mathbf{w}^* \mathbf{b}}$ and $\mathbf{z} \equiv (I - E^*\mathbf{w}\mathbf{v}^*)\frac{\mathbf{c}}{\mathbf{v}^* \mathbf{c}}$, it follows that

$$\mathbf{u} = (\rho_k - \lambda)^{-1}(\rho_k E - A)\mathbf{d}_k \perp \mathbf{w} \quad and \quad \mathbf{z} = (\rho_k - \lambda)^{-*}(\rho_k E - A)^* \mathbf{e}_k \perp \mathbf{v},$$

5

and with $\rho_{k+1} = \mathbf{y}_k^* A \mathbf{x}_k / (\mathbf{y}_k^* E \mathbf{x}_k)$, one has that

$$\rho_{k+1} - \lambda = (\rho_k - \lambda)\mu, \ \ where \ \mu = \frac{\mathbf{e}_k^* \mathbf{u} + \mathbf{e}_k^* E \mathbf{d}_k}{1 + \mathbf{e}_k^* E \mathbf{d}_k}. \tag{9}$$

Note that $\mathbf{u}$ and $\mathbf{z}$ do not change during the iteration.

Proof. Substitution of (8) into (7) and multiplication from the left by $\mathbf{w}^*$ and $\mathbf{v}^*$, respectively, gives

$$\tau_k = \frac{\rho_k - \lambda}{\mathbf{w}^* \mathbf{b}} \ \ \text{and} \ \ \omega_k = \frac{(\rho_k - \lambda)^*}{\mathbf{v}^* \mathbf{c}}.$$

It follows that

$$(\rho_k E - A)\mathbf{d}_k = (\rho_k - \lambda)(I - E\mathbf{v}\mathbf{w}^*)\frac{\mathbf{b}}{\mathbf{w}^* \mathbf{b}} \equiv (\rho_k - \lambda)\mathbf{u} \perp \mathbf{w}$$

and

$$(\rho_k E - A)^* \mathbf{e}_k = (\rho_k - \lambda)^*(I - E^*\mathbf{w}\mathbf{v}^*)\frac{\mathbf{c}}{\mathbf{v}^* \mathbf{c}} \equiv (\rho_k - \lambda)^* \mathbf{z} \perp \mathbf{v},$$

where $\mathbf{u}$ and $\mathbf{z}$ are independent of the iteration. With $\rho_{k+1} = \mathbf{y}_k^* A \mathbf{x}_k / (\mathbf{y}_k^* E \mathbf{x}_k)$, it follows that

$$\rho_{k+1} - \lambda = \frac{\mathbf{y}_k^*(A - \lambda E)\mathbf{x}_k}{\mathbf{y}_k^* E \mathbf{x}_k} = \frac{\mathbf{e}_k^*(A - \lambda E)\mathbf{d}_k}{1 + \mathbf{e}_k^* E \mathbf{d}_k}.$$

Note that $\mathbf{e}_k^*(A - \lambda E)\mathbf{d}_k = \mathbf{e}_k^*(A - \rho_k E)\mathbf{d}_k + (\rho_k - \lambda)\mathbf{e}_k^* E \mathbf{d}_k = (\rho_k - \lambda)(\mathbf{e}_k^* \mathbf{u} + \mathbf{e}_k^* E \mathbf{d}_k)$, which shows (9). $\qquad\square$

Theorem 4.2. *Let $\mathbf{v}$ and $\mathbf{w}$ be right and left eigenvectors of (A, E) with eigenvalue λ, i.e. $(A - \lambda E)\mathbf{v} = 0$ and $\mathbf{w}^*(A - \lambda E) = 0$, and $\mathbf{w}^* E \mathbf{v} = 1$. Then $\lim_{k \to \infty} \mathbf{x}_k = \mathbf{v}$ and $\lim_{k \to \infty} \mathbf{y}_k = \mathbf{w}$ if and only if $s_{k+1} = \rho_k = \rho(\mathbf{x}_k, \mathbf{y}_k)$ approaches λ, and the convergence rate is asymptotically quadratic.*

Proof. The proof is an adaptation of the proofs in [15, p. 689] and [8, p. 150]. The main difference here is that for DPA the right hand-sides of the linear systems are kept fixed during the iterations. Let the iterates $\mathbf{x}_k$ and $\mathbf{y}_k$, see lemma 4.1, be of the form

$$\mathbf{x}_k = \mathbf{v} + \mathbf{d}_k \ \ \text{and} \ \ \mathbf{y}_k = \mathbf{w} + \mathbf{e}_k,$$

where $\mathbf{w}^* E \mathbf{d}_k = \mathbf{e}_k^* E \mathbf{v} = 0$ and $\mathbf{w}^* E \mathbf{v} = 1$. Put $\mathbf{d}_k = (\rho_k - \lambda)\tilde{\mathbf{d}}_k$ with $(\rho_k E - A)\tilde{\mathbf{d}}_k = \mathbf{u}$, and $\mathbf{e}_k = (\rho_k - \lambda)^*\tilde{\mathbf{e}}_k$ with $(\rho_k E - A)^*\tilde{\mathbf{e}}_k = \mathbf{z}$. Since $(\lambda E - A)^{-1} : \mathbf{w}^\perp \to (E^*\mathbf{w})^\perp$ is bounded on $\mathbf{w}^\perp$ and $(\lambda E - A)^{-*} : \mathbf{v}^\perp \to (E\mathbf{v})^\perp$ is bounded on $\mathbf{v}^\perp$, it follows that as $\rho_k \to \lambda$, then

$$||\mathbf{d}_k|| = ||(\rho_k - \lambda)(\rho_k E - A)^{-1}\mathbf{u}|| = |\rho_k - \lambda| ||((\lambda E - A)|_{(E^*\mathbf{w})^\perp})^{-1}|| ||\mathbf{u}|| + O((\rho_k - \lambda)^2), \tag{10}$$

and similarly

$$||\mathbf{e}_k|| = ||(\rho_k - \lambda)^*(\rho_k E - A)^{-*}\mathbf{z}|| = |\rho_k - \lambda| ||((\lambda E - A)|_{(E\mathbf{v})^\perp})^{-*}|| ||\mathbf{z}|| + O((\rho_k - \lambda)^2), \tag{11}$$

and $\mathbf{d}_k$ and $\mathbf{e}_k$, and $\tilde{\mathbf{d}}_k$ and $\tilde{\mathbf{e}}_k$, are bounded. Hence, $\rho_k \to \lambda$ if and only if $\mathbf{x}_k \to \mathbf{v}$ and $\mathbf{y}_k \to \mathbf{w}$.

To prove the asymptotically quadratic rate of convergence, first note that

$$\rho_{k+1} - \lambda = \rho(\mathbf{x}_k, \mathbf{y}_k) = (\rho_k - \lambda)^2 \frac{\tilde{\mathbf{e}}_k^*(A - \lambda E)\tilde{\mathbf{d}}_k}{1 + (\rho_k - \lambda)^2 \tilde{\mathbf{e}}_k^* E \tilde{\mathbf{d}}_k},$$

and hence

$$|\rho_{k+1} - \lambda| = (\rho_k - \lambda)^2 |\tilde{\mathbf{e}}_k^*(A - \lambda E)\tilde{\mathbf{d}}_k| + O((\rho_k - \lambda)^4). \tag{12}$$

6

Let $\kappa(A|_{x^{\perp}})$ denote the condition number of A restricted to $x^{\perp}$. By (10) and (12), it follows that as $k \to \infty$, then

$$
\begin{aligned}
||\mathbf{v} - \mathbf{x}_{k+1}|| &= ||(\rho_{k+1} - \lambda)\tilde{\mathbf{d}}_{k+1}|| \\
&\leq |\rho_k - \lambda|^2 ||\tilde{\mathbf{d}}_k|| ||\tilde{\mathbf{e}}_k|| (\kappa((A - \lambda E)|_{(E^*\mathbf{w})^{\perp}})||\mathbf{u}||) + O((\rho_k - \lambda)^3),
\end{aligned}
$$

and similarly, by (11) and (12),

$$
\begin{aligned}
||\mathbf{w} - \mathbf{y}_{k+1}|| &= ||(\rho_{k+1} - \lambda)\tilde{\mathbf{e}}_{k+1}|| \\
&\leq |\rho_k - \lambda|^2 ||\tilde{\mathbf{e}}_k|| ||\tilde{\mathbf{d}}_k|| (\kappa((A - \lambda E)|_{(E\mathbf{v})^{\perp}})||\mathbf{z}||) + O((\rho_k - \lambda)^3),
\end{aligned}
$$

which proves the asymptotically quadratic convergence. $\qquad\square$

4.2 Convergence neighborhood

In this section it will be assumed that A is a symmetric matrix. In [12] Ostrowski characterizes the convergence neighborhood of the iteration

$$(A - \rho_k I)\mathbf{x}_k = \tau_k \mathbf{b}, \quad k = 0, 1, \ldots, \tag{13}$$

for symmetric matrices A, where ρ_0 arbitrary, $\rho_{k+1} = \rho(A, \mathbf{x}_k)$ $(k > 0)$ and τ_k is a scalar so that $||\mathbf{x}_k||_2 = 1$. It can be seen that DPA for symmetric matrices (with $E = I$, $\mathbf{b} = \mathbf{c}$),

$$(\rho_k I - A)\mathbf{x}_k = \tau_k \mathbf{b}, \quad k = 0, 1, \ldots, \tag{14}$$

is similar and hence Ostrowski's approach can be used to characterize the local convergence neighborhood of DPA for symmetric matrices A with $\mathbf{c} = \mathbf{b} = (b_1, \ldots, b_n)^T$. In fact, a larger convergence neighborhood of DPA will be derived here. This result gives insight in the typical convergence behavior of DPA.

Since the two-sided Rayleigh quotient and (13, 14) are invariant under unitary similarity transforms, without loss of generality A will be a diagonal matrix $\operatorname{diag}(\lambda_1, \ldots, \lambda_n)$ with $\lambda_1 < \ldots < \lambda_n$. Note that $R_j = b_j^2$ and the λ_j with $j = \operatorname{argmax}_j(b_j^2)$ is the dominant pole. The main results of this paper, sharp bounds for the convergence neighborhoods of DPA and RQI, respectively, are stated in theorem 4.3 and theorem 4.4, respectively. The proofs are given in section 4.2.1.

Theorem 4.3. *Let $(\lambda, \mathbf{v})$ be an eigenpair of A. In the DPA iteration for A and $\mathbf{b}$ with initial shift ρ_0, let $\mathbf{x}_k$ and τ_k be such that*

$$||\mathbf{x}_k|| = 1, \quad (\rho_k I - A)\mathbf{x}_k = \tau_k \mathbf{b}, \text{ with } \rho_{k+1} \equiv \mathbf{x}_k^* A \mathbf{x}_k, \quad (k \geq 0),$$

and put $\gamma = \min_{\lambda_i \neq \lambda} |\lambda_i - \lambda|$. If

$$\alpha_{dpa} \equiv \frac{|\rho_0 - \lambda|}{\gamma} \leq \frac{1}{1 + \zeta^2} \text{ with } \zeta \equiv \tan \angle(\mathbf{v}, \mathbf{b}), \tag{15}$$

then, with $c \equiv \cos \angle(\mathbf{v}, \mathbf{b})$, it follows that

$$\rho_k \to \lambda \quad and \quad \frac{|\rho_{k+1} - \lambda|}{c^2 \gamma} \leq \left(\frac{|\rho_k - \lambda|}{c^2 \gamma}\right)^2 \quad (k \geq 0).$$

The bound given by Ostrowski [12, p. 235 (eqn. (19))] is

$$|\rho_k - \lambda| < \frac{\gamma}{2} \min\left(\frac{b^2}{2(1 - b^2)}, 1\right),$$

and it is clear that the neighborhood in theorem 4.3 is larger.

In [12, p. 239] also the convergence neighborhood of standard RQI,

$$(A - \rho_k I)\mathbf{x}_k = \tau_k \mathbf{x}_{k-1}, \quad k = 0, 1, \ldots \tag{16}$$

where $\mathbf{x}_{-1}$ arbitrary, $\rho_{k+1} = \rho(A, \mathbf{x}_k)$ $(k > 0)$ and τ_k is a scalar so that $||\mathbf{x}_k||_2 = 1$, is derived. Here a sharper bound is derived.
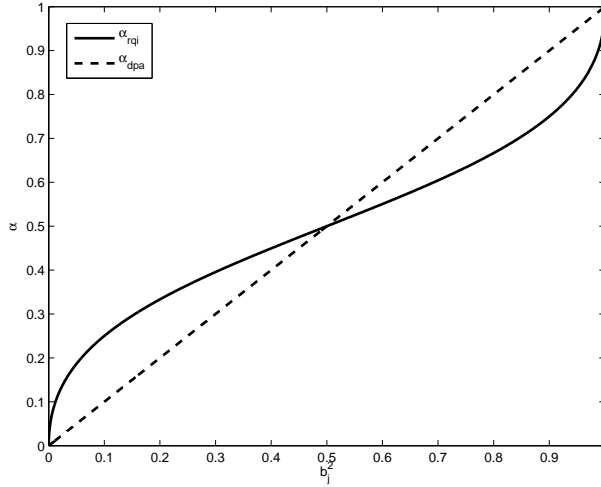
Figure 2: Bounds of the local convergence neighborhood for DPA (dashed) and best-case RQI (solid). If $|\lambda_j - \rho_k| < \alpha\gamma$, with $\gamma = \min_{i \neq j} |\lambda_i - \lambda_j|$, there is convergence to λ_j.

Theorem 4.4. *Let $(\lambda, \mathbf{v})$ be an eigenpair of A. In the RQI iteration for A and $\mathbf{b}$ with initial shift ρ_0 and $\mathbf{x}_{-1} = \mathbf{b}$, let $\mathbf{x}_k$ and τ_k be such that*

$$||\mathbf{x}_k|| = 1, \quad (\rho_k I - A)\mathbf{x}_k = \tau_k \mathbf{x}_{k-1}, \quad \text{with } \rho_{k+1} \equiv \mathbf{x}_k^* A \mathbf{x}_k, \quad (k \geq 0),$$

and put $\gamma = \min_{\lambda_i \neq \lambda} |\lambda_i - \lambda|$. If

$$\alpha_{rqi} \equiv \frac{|\rho_0 - \lambda|}{\gamma} \leq \frac{1}{1+\zeta} \text{ with } \zeta \equiv \tan\angle(\mathbf{v}, \mathbf{b}), \tag{17}$$

then $|\rho_1 - \lambda| < \gamma/2$, and

$$\rho_k \to \lambda \quad and \quad \frac{|\rho_{k+1} - \lambda|}{\gamma - |\rho_{k+1} - \lambda|} \leq \left(\frac{|\rho_k - \lambda|}{\gamma - |\rho_k - \lambda|}\right)^2 \quad (k > 0).$$

In particular, the results of theorem 4.3 and 4.4 are sharp in the sense that if, in the two-dimensional case, condition (15) (condition (17)) is not fulfilled for λ_1, then it is fulfilled for λ_2. This follows from the fact that if $\alpha_0^{(1)} = |\rho_0 - \lambda_1|/\gamma$, then $\alpha_0^{(2)} = 1 - \alpha_0^{(1)}$, and $\zeta_0^{(1)} = 1/\zeta_0^{(2)}$.

In [4][Thm. 1] it is shown that, with $\gamma_b = \beta - \alpha$ a known gap in the spectrum of A (for instance, $\gamma = \min_{\lambda_i \neq \lambda} |\lambda - \lambda_i|$), if $\rho_1 < (\alpha + \beta)/2$ *and* $||\mathbf{r}_1|| = ||A\mathbf{x}_0 - \rho_1\mathbf{x}_0|| \leq \gamma_b$, then $\rho_k < (\alpha + \beta)/2$ for $k \geq 1$, and similarly for the case $\rho_1 > (\alpha + \beta)/2$. It can be shown that the conditions of this theorem imply the second step of theorem 4.4. On the other hand, the conditions of theorem 4.4 do not imply the conditions of [4][Thm. 1]. To see this, consider the two-dimensional example $A = \text{diag}(-1, 1)$. With $\rho_0 = 0.01$, $\mathbf{x}_{-1} = \mathbf{b} = [\sqrt{2}/2, \sqrt{2}/2]$ and $\mathbf{x}_0 = (A - \rho_0 I)^{-1}\mathbf{x}_{-1}$, it follows that $|\lambda - \rho_0| < 1$ and condition (17) is satisfied, while $||\mathbf{r}_1|| = ||A\mathbf{x}_0 - \rho_1\mathbf{x}_0|| \approx 1.03 > 1$. Hence, the result in theorem 4.4 is sharper.

In figure 2, α_{dpa} and α_{rqi}, see equations (15) and (17), respectively, are plotted for $0 < b_j^2 < 1$, $||\mathbf{b}||_2 = 1$. As b_j^2 increases, i.e. as mode j becomes more dominant, both local convergence neighborhoods increase and $\alpha \to 1$, while the bound for the DPA neighborhood is larger for $b^2 > 1/2$, or $\angle(\mathbf{v}, \mathbf{b}) < 45°$.

The price one has to pay for the cubic convergence, is the smaller local convergence neighborhood of the dominant pole, as it becomes more dominant, for RQI. While DPA emphasizes the

8

dominant mode every iteration by keeping the right hand-side fixed, RQI only takes advantage of this in the first iteration, and for initial shifts too far from the dominant pole, the dominant mode may be damped out from the iterates $\mathbf{x}_k$. In that sense, RQI is closer to the inverse power method or inverse iteration, which converges to the eigenvalue closest to the shift, while DPA takes advantage of the information in the right hand-side $\mathbf{b}$.

Because the results are in fact lower bounds for the local convergence neighborhood, theoretically speaking no conclusions can be drawn about the global basins of attraction. But the results strengthen the intuition that for DPA the basin of attraction of the dominant pole is larger than for RQI.

4.2.1   Proofs of theorem 4.3 and theorem 4.4

The following two lemmas provide expressions and bounds that are needed for the proofs of theorem 4.3 and theorem 4.4.

Lemma 4.5. *Let $\mathbf{v}$ be an eigenvector of $A = A^T$ with eigenvalue λ with $||\mathbf{v}|| = 1$, and let $\tau_k \in \mathbb{R}$ be a scaling factor so that the solution $\mathbf{x}_k$ of*

$$(\rho_k I - A)\mathbf{x}_k = \tau_k \mathbf{b}$$

is of the form

$$\mathbf{x}_k = \mathbf{v} + \mathbf{d}_k, \tag{18}$$

where $\mathbf{v}^* \mathbf{d}_k = 0$, and let $\mathbf{z} = (\rho_k E - A)\mathbf{d}_k$. Then $\rho_{k+1} = \mathbf{x}_k^* A \mathbf{x}_k / (\mathbf{x}_k^* \mathbf{x}_k)$ satisfies

$$\rho_{k+1} - \lambda = (\rho_k - \lambda)\mu,$$

where

$$\mu = \frac{\mathbf{d}_k^* \mathbf{z} + \mathbf{d}_k^* \mathbf{d}_k}{1 + \mathbf{d}_k^* \mathbf{d}_k}. \tag{19}$$

Proof. The result follows from lemma 4.1, by noting that $A = A^T$ and $E = I$.   □

Lemma 4.6. *Under the assumptions of lemma 4.5, put $\gamma = \min_{\lambda_i \neq \lambda} |\lambda_i - \lambda|$, $c = \cos \angle(\mathbf{v}, \mathbf{b})$, $\zeta = ||\mathbf{z}||$, $\alpha_k = \frac{|\rho_k - \lambda|}{\gamma}$, and $\tilde{\alpha}_k = \alpha_k / (1 - \alpha_k)$. The following statements hold:*

$$\zeta_{k+1} \equiv ||\mathbf{d}_k|| \leq \frac{\alpha_k}{1 - \alpha_k} \zeta. \tag{20}$$

If $\alpha_k \leq c = 1/\sqrt{1 + \zeta^2}$, then

$$|\mu| \leq \frac{\tilde{\alpha}_k + \tilde{\alpha}_k^2}{1 + \tilde{\alpha}_k^2 \zeta^2} \zeta^2 = \frac{\alpha_k \zeta^2}{(1 - \alpha_k)^2 + \alpha_k^2 \zeta^2}, \tag{21}$$

$$|\mu| \leq 1 \text{ if } \tilde{\alpha}_k \zeta^2 \Leftrightarrow \alpha_k \leq \frac{1}{1 + \zeta^2} = c^2, \tag{22}$$

$$\alpha_{k+1} \leq \alpha_k |\mu| \leq \alpha_k^2 (1 + \zeta^2), \tag{23}$$

$$and \ \tilde{\alpha}_{k+1} \equiv \frac{\alpha_{k+1}}{1 - \alpha_{k+1}} \leq (\tilde{\alpha}_k \zeta)^2. \tag{24}$$

Proof. Put $\zeta_k = ||\mathbf{d}_k||$. Then by (19)

$$|\mu| \leq \phi(\zeta_k) \text{ where } \phi(\tau) \equiv \frac{\zeta \tau + \tau^2}{1 + \tau^2} \quad (\tau \in \mathbb{R}).$$

The function ϕ is increasing on $[0, \tau_{\max}]$, where $\tau_{\max} = (1 + \sqrt{1 + \zeta^2})/\zeta$, or, using $c \equiv \cos \angle(\mathbf{v}, \mathbf{b}) = 1/\sqrt{1 + \zeta^2}$, $\tau_{\max} = \sqrt{(1 + c)/(1 - c)}$, and $0 \leq \phi \leq \frac{1 + c}{2c}$ on $(0, \infty)$.

Since $||(A - \rho_k)^{-1}|_{\mathbf{v}^\perp}|| \leq |1/(\gamma - |\lambda - \rho_k|)|$, it follows that

$$\zeta_k \equiv ||\mathbf{d}_k|| \leq |\rho_k - \lambda| \cdot ||(A - \rho_k)^{-1}|_{\mathbf{v}^\perp}|| \cdot ||\mathbf{z}|| \leq \frac{|\rho_k - \lambda|}{|\gamma - |\rho_k - \lambda||} = \frac{\alpha}{1 - \alpha}\zeta,$$

which proves (20). Statement (21) now follows from the observation that $\alpha_k \zeta/(1 - \alpha) \leq \tau_{\max}$ if and only if $\alpha_k \leq 1/\sqrt{1 + \zeta^2} = c$. Statement (22) follows readily from statement (20) and the definition $\tilde{\alpha}_k = \alpha_k/(1 - \alpha_k)$.

For statement (23), first note that $(1 - \alpha_k)^2 + \alpha_k^2 \zeta^2 \geq \zeta^2/(1 + \zeta^2)$ for all $\alpha_k \geq 0$, and therefore $|\mu| \leq \alpha_k(1 + \zeta^2)$. Hence, with $\alpha_{k+1} \equiv |\rho_{k+1} - \lambda|/\gamma$, inequality (23) follows by (19).

Finally, statement (24) follows the fact that (21) and (24) imply $\alpha_{k+1} \leq (\tilde{\alpha}_k \zeta)^2/(1 + (\tilde{\alpha}_k \zeta)^2)$. $\qquad \square$

Note that it is essential that the function ϕ is increasing, since this allows to use upper bound (20) also to handle the denominator in (19), leading to (21).

In the two-dimensional case, the estimate in (21) is sharp (equality), since both $\mathbf{z}$ and $\mathbf{d}_k$ are in the same direction (orthogonal to $\mathbf{v}$). Furthermore, in statement 2, $|\mu| \leq 1$ if and only if $\tilde{\alpha}_k \zeta^2 \leq 1$.

Proof of theorem 4.3. Note that ζ is the same in all iterations, and recall that $\alpha_k \equiv |\rho_k - \lambda|/\gamma$. Since $c^2 = 1/(1 + \zeta^2)$, condition (15) implies $\alpha_0(1 + \zeta^2) < 1$, and by induction and (23) of lemma 4.6, $\alpha_k\sqrt{1 + \zeta^2} \leq \alpha_k(1 + \zeta^2) < 1$. Again by (23) of lemma 4.6, it follows that

$$\alpha_{k+1}(1 + \zeta^2) \leq (\alpha_k(1 + \zeta^2))^2,$$

which implies the quadratic convergence. $\qquad \square$

Note that result (24) implies $\tilde{\alpha}_{k+1}\zeta^2 \leq (\tilde{\alpha}_k\zeta^2)^2$, which guarantees quadratic convergence as soon as $\tilde{\alpha}_0\zeta^2 < 1$. This condition is equivalent to $\alpha_0 < 1/(1 + \zeta^2)$, the condition (15) of the theorem.

Proof of theorem 4.4. Note that $\zeta_k = \tan\angle(\mathbf{v}, \mathbf{x}_k)$ changes every iteration, and recall that $\alpha_k \equiv |\rho_k - \lambda|/\gamma$, and $\tilde{\alpha}_k = \alpha_k/(1 - \alpha_k)$. Condition (17) implies $\alpha_0 < 1/(1 + \zeta)$, or, equivalently, $\tilde{\alpha}_0\zeta_0 < 1$. By (24) it follows that $\alpha_1 < 1/2$, or, equivalently, $|\rho_1 - \lambda| < \gamma/2$. Since $\tilde{\alpha}_k\zeta_k < 1$ implies that $\alpha_k < 1/\sqrt{1 + \zeta_k^2}$, results (20) and (24) of lemma 4.6 can be applied to obtain

$$\tilde{\alpha}_{k+1} \leq (\tilde{\alpha}_k\zeta_k)^2 \quad \text{and} \quad \zeta_{k+1} \leq \tilde{\alpha}_k\zeta_k,$$

if $\tilde{\alpha}_k\zeta_k < 1$. It follows that $\zeta_{k+2} \leq \tilde{\alpha}_{k+1}\zeta_{k+1} \leq (\tilde{\alpha}_k\zeta_k)^3 < 1$. Therefore, since $\tilde{\alpha}_0\zeta_0 < 1$, the sequences $(\tilde{\alpha}_k)$ and (ζ_k) converge dominated cubically, and, for $k > 0$, $\tilde{\alpha}_{k+1} \leq \tilde{\alpha}_k^2$. $\qquad \square$

4.3 General systems

Theorems 4.3 and 4.4 can readily be generalized for normal matrices, but it is difficult to obtain such bounds for general matrices without making specific assumptions. To see this, note that it is difficult to give sharp bounds for (9) in lemma 4.1. However, the following theorem states that DPA is invariant under certain transformations and helps in getting more insight in DPA for general, non-defective systems $(E, A, \mathbf{b}, \mathbf{c})$.

Theorem 4.7. *Let (A, E) be a non-defective matrix pencil, and let $X, Y \in \mathbb{C}^{n \times n}$ be of full rank. If $DPA(E, A, \mathbf{b}, \mathbf{c}, s_0)$ produces the sequence $(\mathbf{x}_k, \mathbf{y}_k, s_{k+1})$, then $DPA(Y^*EX, Y^*AX, Y^*\mathbf{b}, X^*\mathbf{c}, s_0)$ produces the sequence $(X^{-1}\mathbf{x}_k, Y^{-1}\mathbf{y}_k, s_{k+1})$, and vice versa.*

Proof. If $\mathbf{x} = \mathbf{x}_k$ is the solution of

$$(sE - A)\mathbf{x} = \mathbf{b},$$

then $\tilde{\mathbf{x}} = \tilde{\mathbf{x}}_k = X^{-1}\mathbf{x}$ is the solution of

$$(sY^*EX - Y^*AX)\tilde{\mathbf{x}} = Y^*\mathbf{b},$$

10

and vice versa. Similar relations hold for $\mathbf{y} = \mathbf{y}_k$ and $\tilde{\mathbf{y}} = \tilde{\mathbf{y}}_k = Y^{-1}\mathbf{y}$. The proof is completed by noting that

$$s_{k+1} = \frac{\tilde{\mathbf{y}}^* Y^* A X \tilde{\mathbf{x}}}{\tilde{\mathbf{y}}^* Y^* E X \tilde{\mathbf{x}}} = \frac{\mathbf{y}^* A \mathbf{x}}{\mathbf{y}^* E \mathbf{x}} = s_{k+1}.$$

$\square$

Let W and V have as their columns the left and right eigenvectors of (A, E), respectively, i.e. $AV = EV\Lambda$ and $W^* A = \Lambda W^* E$, with $\Lambda = \mathrm{diag}(\lambda_1, \ldots, \lambda_n)$. Furthermore, let W and V be scaled so that $W^* E V = \Delta$, where Δ is a diagonal matrix with $\delta_{ii} = 1$ for finite λ_i and $\delta_{ii} = 0$ for $|\lambda_i| = \infty$. According to theorem 4.7, DPA$(E, A, \mathbf{b}, \mathbf{c})$ and DPA$(\Delta, \Lambda, W^*\mathbf{b}, V^*\mathbf{c})$ produce the same pole estimates s_k. In $\tilde{\mathbf{b}} = W^*\mathbf{b}$ and $\tilde{\mathbf{c}} = V^*\mathbf{c}$, the new right hand-sides, one recognizes the contributions to the residues $R_i = \tilde{\mathbf{c}}_i \tilde{\mathbf{b}}_i = (\mathbf{c}^* \mathbf{v}_i)(\mathbf{w}_i^* \mathbf{b})$. The more dominant pole λ_i is, the larger the corresponding coefficients $\tilde{\mathbf{b}}_i$ and $\tilde{\mathbf{c}}_i$ are, and, since (Λ, Δ) is a diagonal pencil, the larger the chance that DPA converges to the unit vectors $\tilde{\mathbf{v}} = \mathbf{e}_i$ and $\tilde{\mathbf{w}} = \mathbf{e}_i$, that correspond to the right and left eigenvectors $\mathbf{v}_i = V\mathbf{e}_i$ and $\mathbf{w}_i = W\mathbf{e}_i$, respectively.

As observed earlier, DPA emphasizes the dominant mode every iteration by keeping the right hand-sides fixed, and thereby can be expected to enlarge the convergence neighborhood also for general systems, compared to two-sided RQI. In practice, the quadratic instead of cubic rate of local convergence costs at most 2 or 3 iterations. Numerical experiments confirm that the basins of attraction of the dominant eigenvalues are larger for DPA, as will be discussed in the following section.

5 Basins of attraction and typical convergence behavior

It is not straightforward to characterize the global convergence of DPA, even not for symmetric matrices (see [12, p. 236-237]). Basins of attraction of RQI in the three-dimensional case are studied in [1, 3, 14], while in [4, 21] local convergence neighborhoods are described. Because the DPA residuals $\mathbf{r}_k = (A - \rho_k I)\mathbf{b}$ are not monotonically decreasing (in contrast to the inverse iteration residuals $\mathbf{r}_k = (A - \sigma I)\mathbf{x}_k$ and the RQI residuals $\mathbf{r}_k = (A - \rho_k I)\mathbf{x}_k$, see [4, 14, 15]), it is not likely that similar results can be obtained for DPA. Numerical experiments, however, may help to get an idea of the typical convergence behavior of DPA and may show why DPA is to be preferred over two-sided RQI for the computation of dominant poles.

An unanswered question is how to choose the initial shift of DPA. An obvious choice is the two-sided Rayleigh quotient $s_0 = (\mathbf{c}^* A \mathbf{b})/(\mathbf{c}^* E \mathbf{b})$. This choice will work in the symmetric case $A = A^*, E = I, \mathbf{c} = \mathbf{b}$. In the general nonsymmetric case this choice will not always be possible: the vectors $\mathbf{b}$ and $\mathbf{c}$ are often very sparse (only $O(1)$ nonzero entries) and moreover, it may happen that $\mathbf{c}^* E \mathbf{b} = 0$. In that case the initial shift should be based on heuristics. For two-sided RQI, an obvious choice is to take as the initial vectors $\mathbf{x}_0 = \mathbf{b}$ and $\mathbf{y}_0 = \mathbf{c}$, but similarly, if $\mathbf{y}_0^* E \mathbf{x}_0 = 0$, this fails. Therefore, in the following experiments an initial shift s_0 will be chosen and the (normalized) initial vectors for two-sided RQI are $\mathbf{x}_0 = (A - s_0 E)^{-1}\mathbf{b}$ and $\mathbf{y}_0 = (A - s_0 E)^{-1}\mathbf{c}$, see Alg. 2.

All experiments were executed in Matlab 7 [22]. The criterion for convergence was $||A\mathbf{x}_k - s_{k+1} E \mathbf{x}_k||_2 < 10^{-8}$.

5.1 Three-dimensional symmetric matrices

Because RQI and DPA are shift and scaling invariant, the region of all 3×3 symmetric matrices can be parametrized by $A = \mathrm{diag}(-1, s, 1)$, with $0 \le s < 1$ due to symmetry (see [14]). In order to compute the regions of convergence of RQI and DPA (as defined in (13, 14)), the algorithms are applied to A for initial shifts in the range $(-1, 1) \backslash \{s\}$, with $\mathbf{c} = \mathbf{b} = (b_1, b_2, b_3)^T$, where $0 < b_2 \le 1$ and $b_1 = b_3 = \sqrt{(1 - b_2^2)/2}$. In figure 3 the results are shown for $s = 0$ and $s = 0.8$. The intersections $\rho = \rho_{\lambda_1}$ and $\rho = \rho_{\lambda_3}$ at $b_2 = b$ with the borders define the convergence regions: for $-1 \le \rho_0 < \rho_{\lambda_1}$ there is convergence to $\lambda_1 = -1$, for $\rho_{\lambda_1} \le \rho_0 < \rho_{\lambda_3}$ there is convergence to $\lambda_2 = s$, while for $\rho_{\lambda_3} \le \rho_0 \le 1$ there is convergence to $\lambda_3 = 1$.
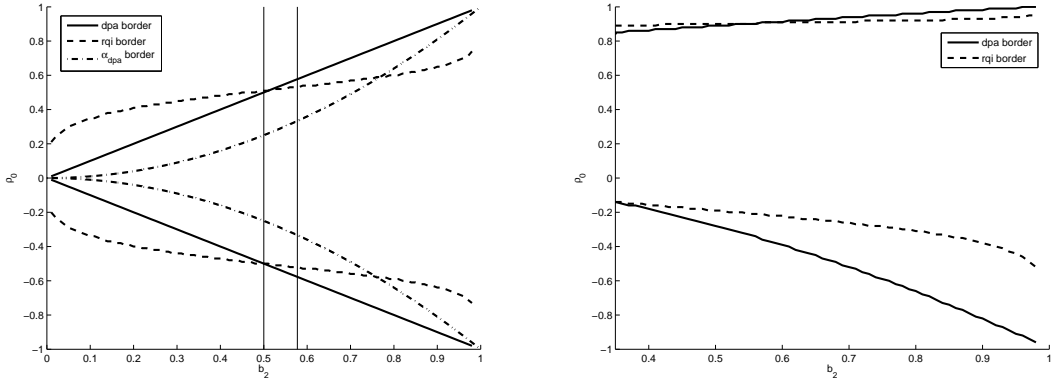
11

Figure 3: Convergence regions for DPA (solid borders) and RQI (dashed), and the theoretical DPA border (dash-dot, see Thm. 4.3), for the matrix $A = \mathrm{diag}(-1, s, 1)$, for $s = 0$ (left) and $s = 0.8$. The regions of convergence to $\lambda_2 = s$ for DPA and RQI respectively are enclosed between the lower and upper borders of DPA and RQI respectively. The regions of convergence to $\lambda_1 = -1$ ($\lambda_3 = 1$) are below (above) the lower (upper) border.

For the case $s = 0$ it can be observed that (see vertical lines) for $0 \leq b_2 \lesssim 0.5$, the convergence region to the dominant extremal eigenvalues is larger for DPA. For $0.5 \lesssim b_2 \leq 1/\sqrt{3} \approx 0.577$, the point at which λ_2 becomes dominant, the convergence region of RQI is larger. However, for $b_2 \gtrsim 0.5$, the convergence region of λ_2 is clearly larger for DPA. Note also that the theoretical (lower bound $\alpha_{dpa}\gamma$ of the) local convergence neighborhood for DPA (Thm. 4.3) is even larger than the practical convergence neighborhood of two-sided RQI for $b_2 \gtrsim 0.8$.

A similar observation can be made for the case $s = 0.8$. There, due to the decentralized location of λ_2, the figure is not symmetric and the region of convergence of λ_2 is clearly larger for DPA. For $0 \leq b_2 \lesssim 0.35$, DPA and RQI appear to be very sensitive to the initial shift. While the convergence region for λ_1 was similar to the case $s = 0$, convergence for $-0.1 \lesssim \rho_0 \lesssim 0.8$ was irregular in the sense that for initial shifts in this interval both λ_2 and λ_3 could be computed; hence the regions are only shown for $b_2 \gtrsim 0.35$. Because the theoretical lower bounds are much smaller, since $d = \min_{i \neq j} |\lambda_i - \lambda_j| = 0.2$, and make the figure less clear, they are not shown (the theoretical DPA border still crosses the practical two-sided RQI border around $b_2 \approx 0.9$).

It is almost generic, that apart from a small interval of values of b_2, the area of convergence of the dominant eigenvalue is larger for DPA than for RQI. The following example discusses a large scale general system.

5.2   A large scale example

This example is a test model of the Brazilian Interconnect Power System (BIPS) [17, 16]. The sparse matrices A and E are of dimension $n = 13,251$ and E is singular. The input and output vectors $\mathbf{b}$ and $\mathbf{c}$ only have one nonzero entry and furthermore $\mathbf{c}^T E \mathbf{b} = 0$; the choice $\mathbf{x}_0 = \mathbf{b}$ and $\mathbf{y}_0 = \mathbf{c}$ is not practical, see the beginning of this section. The pencil (A, E) is non-normal and the most dominant poles appear in complex conjugated pairs. It is not feasible to determine the converge regions for the entire complex plane, but the convergence behavior in the neighborhood of a dominant pole can be studied by comparing the found poles for a number of initial shifts in the neighborhood of the pole, for both DPA and two-sided RQI (Alg. 1 and Alg. 2). The results, for two areas of the complex plane, are shown in figure 4 and figure 5.

Initial shifts for which DPA and two-sided RQI converge to the target (the most dominant pole, in the center of the domain) or its complex conjugate are marked by a circle and an x, respectively. In figure 4, occasionally there is converge to a more dominant pole outside the
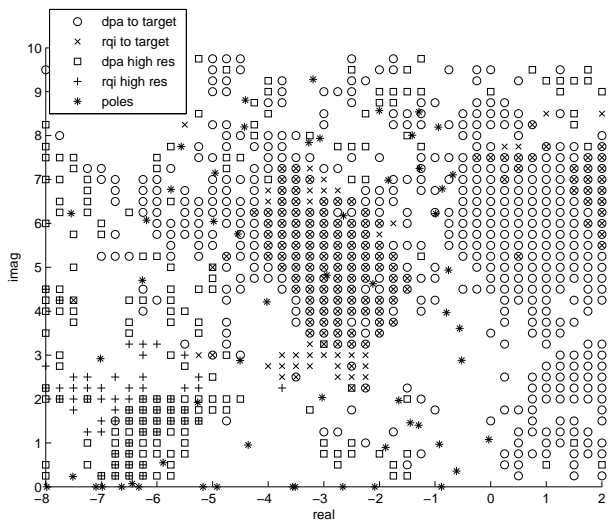
12

Figure 4: Convergence regions for DPA and two-sided RQI, for the example of section 5.2. The center of the domain is the pole $\lambda \approx -2.9 \pm 4.8i$ with residue norm $|R| \approx 3.0 \cdot 10^{-3}$. Circles (x-es) mark initial shifts for which convergence to the target takes place for DPA (two-sided RQI). Horizontal and vertical stride are both 0.25.
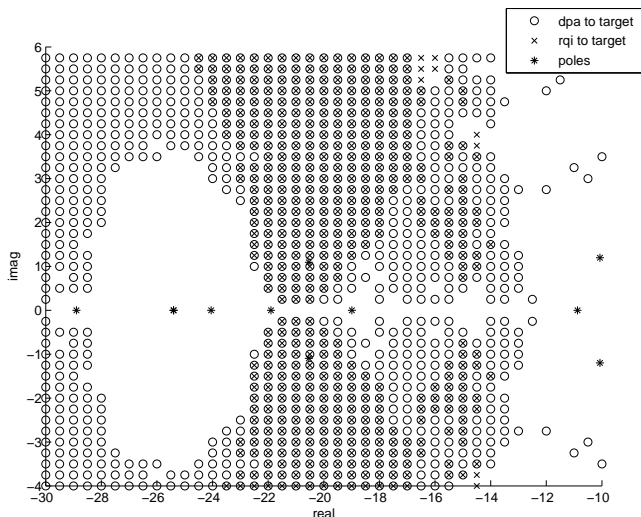

Figure 5: Convergence regions for DPA and two-sided RQI, for the example of section 5.2. The center of the domain is the pole $\lambda \approx -20.5 \pm 1.1i$, with residue norm $|R| \approx 6.2 \cdot 10^{-3}$. Circles (x-es) mark initial shifts for which convergence to the target takes place for DPA (two-sided RQI). Horizontal and vertical stride are 0.5 and 0.25.

depicted area (marked by a square and a +, respectively). Grid points with no marker denote convergence to a less dominant pole.

Figure 4 shows rather irregular convergence regions for both DPA and two-sided RQI. This is caused by the presence of many other (less) dominant poles in this part of the complex plane. Nevertheless, the basins of attraction of the dominant poles are notably larger for DPA. Moreover, it can be observed that even for initial shifts very close to another less dominant pole, DPA converges to a more dominant pole, while two-sided RQI converges to the nearest pole. For example, for initial shift $s_0 = -2 + 4.5i$, DPA converges to $\lambda \approx -2.9 + 4.8i$ with $|R| \approx 3.0 \cdot 10^{-3}$, while two-sided RQI converges to $\lambda \approx -2.1 + 4.6i$ with $|R| \approx 1.0 \cdot 10^{-5}$.

In figure 5 the target is the most dominant pole of the system. It can be clearly observed that for DPA the number of initial shifts that converge to the dominant pole is larger than for two-sided RQI. The basin of attraction of the dominant pole is larger for DPA: except for regions in the neighborhood of other relatively dominant poles (see, for instance, the poles in the interval $(-28, -24)$ on the real axis), there is convergence to the most dominant pole. For DPA typically the size of the basin of attraction increases with the relative dominance of the pole, while for two-sided RQI the effect is less strong, cf. theorem 4.3, theorem 4.4 and the discussion in section 4.2. The symmetry with respect to the real axis can be explained by the fact that if for initial shift s_0, DPA (two-sided RQI) produces the sequence $(\mathbf{x}_k, \mathbf{y}_k, s_{k+1})$ converging to $(\mathbf{v}, \mathbf{w}, \lambda)$, then for $\bar{s}_0$ it produces the sequence $(\bar{\mathbf{x}}_k, \bar{\mathbf{y}}_k, \bar{s}_{k+1})$ converging to $(\bar{\mathbf{v}}, \bar{\mathbf{w}}, \bar{\lambda})$.

In both figures it can be seen that for many initial shifts DPA converges to the most dominant pole, but two-sided RQI does not. On the other hand, for a very small number of initial shifts, two-sided RQI converges to the most dominant pole while DPA does not. This is a counterexample for the obvious thought that if two-sided RQI converges to the dominant pole, then also DPA converges to it.

The average number of iterations needed by DPA to converge to the most dominant pole was 7.2, while two-sided RQI needed an average number of 6.0 iterations. The average numbers over the cases where both DPA and two-sided RQI converged to the most dominant pole were 6.1 and 5.9 iterations, respectively.

Similar behavior is observed for other systems and transfer functions. Although the theoretical and experimental results do not provide hard evidence in the sense that they prove that the basin of attraction of the dominant pole is larger for DPA than for two-sided RQI, they indicate at least an advantage of DPA over two-sided RQI.

5.3 PEEC example

The PEEC system [6] is a well known benchmark system for model order reduction applications. One of the difficulties with this system of order $n = 584$ is that it has many equally dominant poles that lie close to each other in a relatively small part, $[-1, 0] \times [-10i, 10i]$, of the complex plane. This explains why in figure 6 for only a relatively small part of the plane there is convergence (marked by circles and x-es for DPA and two-sided RQI, respectively) to the most dominant pole $\lambda \approx -0.14 \pm 5.4i$ (marked by a $*$).

Although the difference is less pronounced than in the previous examples, DPA still converges to the most dominant pole in more cases than two-sided RQI, and the average residue norm of the found poles was also larger: $R_{avg}^{dpa} \approx 5.2 \cdot 10^{-3}$ vs. $R_{avg}^{rqi} \approx 4.5 \cdot 10^{-3}$. Again a remarkable observation is that even for some initial shifts very close to another pole, DPA converges to the most dominant pole, while two-sided RQI converges to the nearest pole: e.g., for initial shift $s_0 = 5i$ DPA converges to the most dominant pole $\lambda \approx -0.143 + 5.38i$ with $|R| \approx 7.56 \cdot 10^{-3}$, while two-sided RQI converges to less dominant pole $\lambda \approx -6.3 \cdot 10^{-3} + 4.99i$ with $|R| \approx 3.90 \cdot 10^{-5}$.

The average number of iterations needed by DPA to converge to the most dominant pole was 9.8, while two-sided RQI needed an average number of 7.9 iterations. The average numbers over the cases where both DPA and two-sided RQI converged to the most dominant pole were 9.4 and 7.7 iterations, respectively.
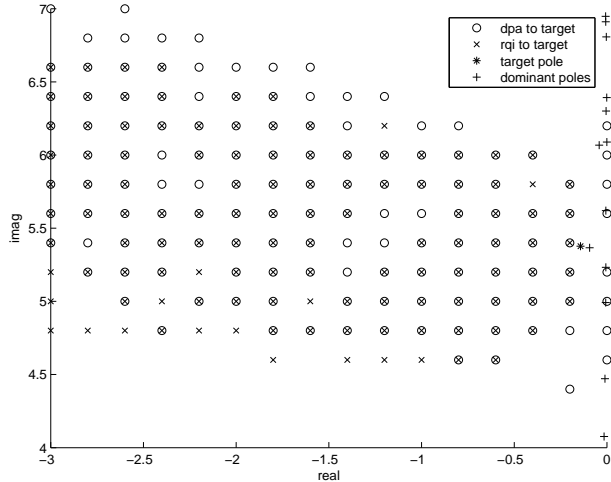
Figure 6: Convergence regions for DPA and two-sided RQI. The center of the domain is the pole $\lambda \approx -0.14 \pm 5.4i$, with residue norm $|R| \approx 7.6 \cdot 10^{-3}$. Circles (x-es) mark initial shifts for which convergence to the target takes place for DPA (two-sided RQI). Horizontal and vertical stride are both 0.2.

6   Conclusions

The theoretical and numerical results confirm the intuition, and justify the conclusion, that the Dominant Pole Algorithm has better global convergence than two-sided Rayleigh quotient iteration to the dominant poles of a large scale dynamical system. The derived local convergence neighborhoods of dominant poles are larger for DPA, as the poles become more dominant, and numerical experiments indicate that the local basins of attraction of the dominant poles are larger for DPA than for two-sided RQI.

Both DPA and two-sided RQI need to solve two linear systems at every iteration. The difference between DPA and two-sided RQI is that DPA keeps the right hand-sides fixed to the input and output vector of the system, while two-sided RQI updates the right hand-sides every iteration. The more dominant a pole is, the bigger the difference in convergence behavior between DPA and two-sided RQI. The other way around, for considerably less dominant poles, the basins of attraction are much smaller for DPA than for two-sided RQI. This could be observed in cases where the initial shift was very close to a less dominant pole and DPA converged to a more dominant pole, while two-sided RQI converged to the nearest, less dominant pole.

The fact that DPA has a asymptotically quadratic rate of convergence, against a cubic rate for two-sided RQI, is of minor importance, since this has only a very local effect and hence leads to a small difference in the number of iterations (typically a difference of 1 or 2 iterations). Furthermore, there exist criteria to switch from DPA to two-sided RQI.

Acknowledgments

15

References

[1] ABSIL, P. A., SEPULCHRE, R., VAN DOOREN, P., AND MAHONY, R. Cubically convergent iterations for invariant subspace computation. *SIAM J. Matrix Anal. Appl. 26*, 1 (2004), 70–96.

[2] AGUIRRE, L. A. Quantitative Measure of Modal Dominance for Continuous Systems. In *Proc. of the 32nd Conference on Decision and Control* (December 1993), pp. 2405–2410.

[3] BATTERSON, S., AND SMILLIE, J. The dynamics of Rayleigh quotient iteration. *SIAM J. Num. Anal. 26*, 3 (June 1989), 624–636.

[4] BEATTIE, C., AND FOX, D. W. Localization criteria and containment for Rayleigh quotient iteration. *SIAM J. Matrix Anal. Appl. 10*, 1 (Januari 1989), 80–93.

[5] BEZERRA, L. H. Written discussion to [10]. *IEEE Trans. Power Syst. 11*, 1 (Feb 1996), 168.

[6] CHAHLAOUI, Y., AND VAN DOOREN, P. A collection of Benchmark examples for model reduction of linear time invariant dynamical systems. SLICOT Working Note 2002-2, 2002.

[7] GREEN, M., AND LIMEBEER, D. J. N. *Linear Robust Control*. Prentice-Hall, 1995.

[8] HOCHSTENBACH, M. E., AND SLEIJPEN, G. L. G. Two-sided and alternating Jacobi-Davidson. *Lin. Alg. Appl. 358*, 1-3 (2003), 145–172.

[9] KAILATH, T. *Linear Systems*. Prentice-Hall, 1980.

[10] MARTINS, N., LIMA, L. T. G., AND PINTO, H. J. C. P. Computing dominant poles of power system transfer functions. *IEEE Trans. Power Syst. 11*, 1 (Feb 1996), 162–170.

[11] MARTINS, N., AND QUINTÃO, P. E. M. Computing dominant poles of power system multivariable transfer functions. *IEEE Trans. Power Syst. 18*, 1 (Feb 2003), 152–159.

[12] OSTROWSKI, A. M. On the convergence of the Rayleigh quotient iteration for the computation of the characteristic roots and vectors. I. *Arch. Rational Mech. Anal. 1* (1958), 233–241.

[13] OSTROWSKI, A. M. On the convergence of the Rayleigh quotient iteration for the computation of the characteristic roots and vectors. III. *Arch. Rational Mech. Anal. 3* (1959), 325–340.

[14] PANTAZIS, R. D., AND SZYLD, D. B. Regions of convergence of the rayleigh quotient iteration method. *Num. Lin. Alg. Appl. 2*, 3 (1995), 251–269.

[15] PARLETT, B. N. The Rayleigh quotient iteration and some generalizations for nonnormal matrices. *Math. Comp. 28*, 127 (July 1974), 679–693.

[16] ROMMES, J., AND MARTINS, N. Efficient computation of multivariable transfer function dominant poles using subspace acceleration. Preprint 1344, Utrecht University, Jan. 2006. Accepted for publication in IEEE Trans. Power Syst.

[17] ROMMES, J., AND MARTINS, N. Efficient computation of transfer function dominant poles using subspace acceleration. *IEEE Trans. Power Syst. 21*, 3 (Aug. 2006), 1218–1226.

[18] SLEIJPEN, G. L. G., AND VAN DER VORST, H. A. A Jacobi-Davidson iteration method for linear eigenvalue problems. *SIAM J. Matrix Anal. Appl. 17*, 2 (1996), 401–425.

[19] SMITH, J. R., HAUER, J. F., TRUDNOWSKI, D. J., FATEHI, F., AND WOODS, C. S. Transfer function identification in power system application. *IEEE Trans. Power Syst. 8*, 3 (Aug 1993), 1282–1290.

[20] STATHOPOULOS, A. A case for a biorthogonal Jacobi-Davidson method: Restarting and correction equation. *SIAM J. Matrix Anal. Appl. 24*, 1 (2002), 238–259.

[21] SZYLD, D. Criteria for combining inverse and Rayleigh quotient iteration. *SIAM J. Num. Anal. 25*, 6 (December 1988), 1369–1375.

[22] THE MATHWORKS, INC. Matlab.

[23] VARGA, A. Enhanced modal approach for model reduction. *Math. Mod. Syst.*, 1 (1995), 91–105.